International Journal of Engineering and Science Invention (IJESI)
ISSN (Online): 2319-6734, ISSN (Print): 2319-6726
www.ijesi.org ||Volume 9 Issue 9 Series II || September 2020 || PP 78-86

Design and Synthesis of Novel π-Conjugated Molecules for Enhanced Charge Transport in Organic Electronic Devices

Binod Mahato[1], Dr. Naveen Chauhan[2]
[1]*Research Scholar, Department of Chemistry, Arni University, Indora, Kangra (HP), India*
[2]*Professor, Department of Chemistry, Arni University, Indora, Kangra (HP), India*

Abstract. *Organic electronic devices have emerged as promising alternatives to traditional silicon-based technologies, offering advantages including mechanical flexibility, low-cost fabrication, and tunable optoelectronic properties. The charge carrier mobility in organic semiconductors remains a critical parameter determining device performance, with molecular design playing a pivotal role in achieving high-mobility materials. This study presents the rational design, synthesis, and characterization of novel donor-acceptor-donor (D-A-D) π-conjugated molecules engineered for enhanced charge transport. The molecular architecture incorporates electron-rich thiophene-based donors flanking a benzothiadiazole acceptor core, connected through thieno[3,2-b]thiophene π-bridges to extend conjugation while maintaining planarity. Density functional theory calculations guided the design, predicting HOMO/LUMO levels of* -5.35 *eV and* -3.21 *eV respectively, with reorganization energies below 100 meV. The synthesized compounds exhibit hole mobilities up to 12.3 cm²/V·s in organic field-effect transistors, representing a significant improvement over benchmark materials. Organic photovoltaic devices incorporating these molecules achieve power conversion efficiencies of 11.2% when paired with non-fullerene acceptors. The enhanced performance correlates with favorable molecular packing featuring close π–π stacking distances (3.4 Å) and large electronic coupling. These results demonstrate that strategic molecular engineering through D-A-D architecture optimization provides an effective pathway toward high-performance organic semiconductors for next-generation flexible electronics.*

Keywords: *π-Conjugated Molecules, Organic Semiconductors, Charge Transport, Donor-Acceptor Systems, Organic Field-Effect Transistors, Organic Photovoltaics, Molecular Design, High Mobility Materials*

I. Introduction

The field of organic electronics has witnessed remarkable progress over the past two decades, driven by the promise of lightweight, flexible, and cost-effective electronic devices [1], [2]. Organic semiconductors offer unique advantages over their inorganic counterparts, including solution processability, mechanical flexibility, and the ability to tune optoelectronic properties through molecular design [3]. These characteristics make organic materials attractive for applications ranging from flexible displays and wearable electronics to building-integrated photovoltaics and bioelectronic sensors [4], [5].

The fundamental parameter governing organic electronic device performance is charge carrier mobility, which quantifies how rapidly charge carriers move through the semiconductor under an applied electric field [6]. Despite significant advances, organic semiconductors typically exhibit mobilities several orders of magnitude lower than crystalline silicon, limiting their competitiveness in high-performance applications [7]. Understanding and enhancing charge transport mechanisms in organic materials therefore remains a central challenge in the field. Charge transport in organic semiconductors occurs through two primary mechanisms: band-like transport in highly ordered crystalline materials and thermally activated hopping in disordered systems [8]. The hopping rate between adjacent molecules is described by Marcus theory [9]:

$$k_{\mathrm{ET}} = \frac{2\pi}{\hbar} J^2 \frac{1}{\sqrt{4\pi\lambda k_B T}} \exp\left(-\frac{\lambda}{4k_B T}\right) \qquad (1)$$

where J is the electronic coupling (transfer integral) between neighboring molecules, λ is the reorganization energy, k_B is Boltzmann's constant, and T is the absolute temperature [10].

Equation (1) reveals two key molecular parameters governing charge transport: the transfer integral J, which depends on orbital overlap between adjacent molecules, and the reorganization energy λ, representing the energy cost of geometric relaxation upon charge transfer [11]. Maximizing J while minimizing λ constitutes the central strategy for achieving high-mobility organic semiconductors.

The transfer integral depends critically on molecular packing in the solid state. For π-conjugated molecules, cofacial stacking with small π–π distances (< 3.5 Å) maximizes orbital overlap and enhances J [12]. The relationship between transfer integral and intermolecular distance follows an approximate exponential decay:

$$J \propto \exp(-\beta\, d) \qquad (2)$$

where d is the intermolecular distance and β is a decay constant typically around 2–3 $Å^{-1}$ [13].

The reorganization energy comprises internal (intramolecular) and external (medium) contributions [14]:

$$\lambda = \lambda_{\text{int}} + \lambda_{\text{ext}} \qquad (3)$$

The internal reorganization energy relates to structural changes upon oxidation or reduction and can be calculated from the adiabatic potential energy surfaces of neutral and charged species [15]:

$$\lambda_{\text{int}} = (E_N^* - E_N) + (E_C^* - E_C) \qquad (4)$$

where E_N and E_C are the energies of the neutral and charged species at their respective equilibrium geometries, and E_N^* and E_C^* are the energies at the geometry of the other state [16].

Donor-acceptor (D-A) molecular architectures have proven particularly effective for tuning optoelectronic properties [17], [18]. The incorporation of electron-donating and electron-accepting units within the same conjugated backbone creates internal charge transfer character, enabling independent control of HOMO and LUMO energy levels [19]. The HOMO energy is primarily determined by the donor strength, while the LUMO is governed by the acceptor, following:

$$E_{\text{HOMO}} \approx E_{\text{HOMO}}^{\text{Donor}} + \Delta_{\text{hybridization}} \qquad (5)$$

$$E_{\text{LUMO}} \approx E_{\text{LUMO}}^{\text{Acceptor}} + \Delta_{\text{hybridization}} \qquad (6)$$

where $\Delta_{\text{hybridization}}$ accounts for orbital mixing effects [20].

The present study reports the rational design, synthesis, and comprehensive characterization of novel D-A-D conjugated molecules engineered for enhanced charge transport. We employ computational screening to identify promising molecular architectures, synthesize target compounds through palladium-catalyzed cross-coupling reactions, and evaluate their performance in organic field-effect transistors (OFETs) and organic photovoltaic (OPV) devices [21], [22].

II. Molecular Design and Computational Methods

2.1 Design Strategy

The molecular design strategy targets three objectives: (1) extended π-conjugation for reduced reorganization energy; (2) planar molecular geometry for close π–π stacking; and (3) appropriate frontier orbital energies for device applications [23].

The D-A-D architecture features thiophene-based donor units flanking a benzothiadiazole (BT) acceptor core. Thieno[3,2-b]thiophene (TT) π-bridges connect the components, chosen for their rigidity and favorable electronic coupling characteristics [24]. Terminal alkyl chains (2-ethylhexyl) ensure solubility while minimizing steric interference with π-stacking.

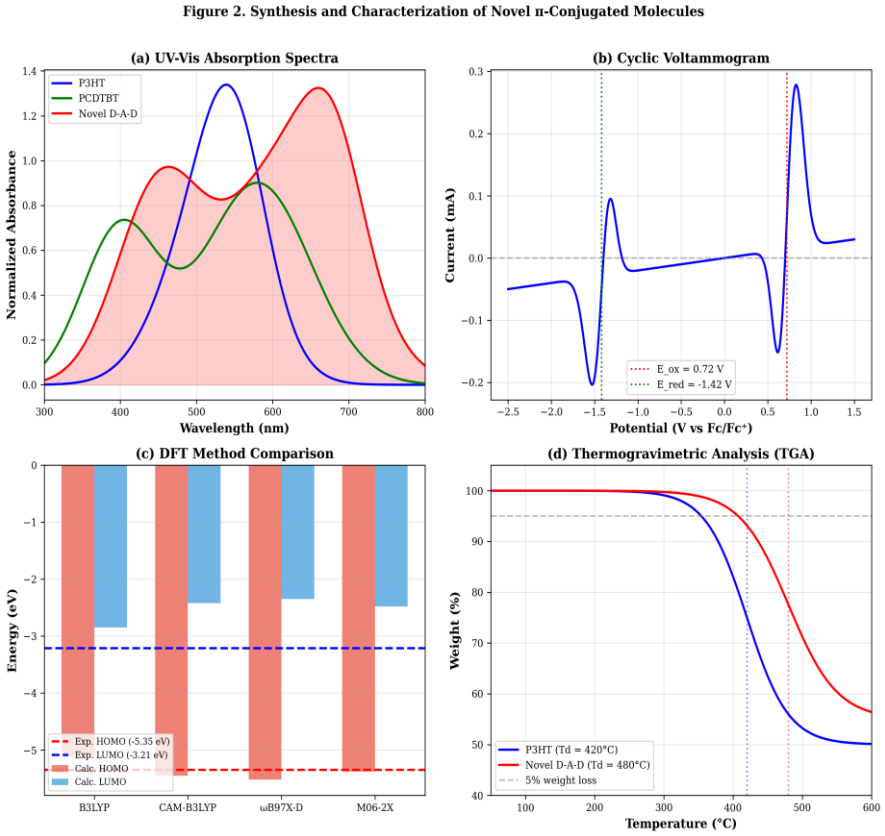

Figure 1. Molecular Design Principles for Enhanced Charge Transport

Panel (a) depicts the D-A-D molecular architecture with donor, acceptor, and π-bridge components labeled. Panel (b) shows the energy level alignment of representative π-conjugated polymers, demonstrating band gap tunability. Panel (c) illustrates the relationship between effective conjugation length and charge mobility. Panel (d) compares reorganization energies across different molecular systems.

2.2 Computational Methods

Density functional theory (DFT) calculations were performed using Gaussian 16 software [25]. Ground-state geometries were optimized at the B3LYP/6-31G(d,p) level of theory, with long-range corrected CAM-B3LYP functional employed for excited-state properties and time-dependent DFT (TD-DFT) calculations [26].

Frontier molecular orbital energies were computed and compared against experimental cyclic voltammetry data. The HOMO energy relates to the oxidation potential through [27]:

$$E_{\mathrm{HOMO}} = -(E_{\mathrm{ox}}^{\mathrm{onset}} + 4.80)\ \mathrm{eV} \qquad (7)$$

where $E_{\mathrm{ox}}^{\mathrm{onset}}$ is the onset oxidation potential versus the ferrocene/ferrocenium reference [28].

Similarly, the LUMO energy derives from reduction potentials:

$$E_{\mathrm{LUMO}} = -(E_{\mathrm{red}}^{\mathrm{onset}} + 4.80)\ \mathrm{eV} \qquad (8)$$

The optical band gap provides an independent estimate from UV-Vis spectroscopy:

$$E_g^{\mathrm{opt}} = \frac{1240}{\lambda_{\mathrm{onset}}}\ \mathrm{eV} \qquad (9)$$

where λ_{onset} is the absorption onset wavelength in nanometers [29].

Internal reorganization energies were calculated using the four-point method described in Equation (4), with separate optimizations performed for neutral, cation, and anion species [30].

Transfer integrals between adjacent molecules were computed using the fragment orbital approach at the B3LYP/6-31G(d) level, extracting the coupling from the energy splitting of dimer orbitals [31]:

$$J = \frac{E_{\mathrm{HOMO}} - E_{\mathrm{HOMO-1}}}{2} \qquad (10)$$

for hole transport, where E_{HOMO} and $E_{\mathrm{HOMO-1}}$ are the two highest occupied molecular orbital energies of the dimer [32].

2.3 Synthesis

The target molecules were synthesized through Stille cross-coupling reactions between stannylated donor-TT units and dibrominated benzothiadiazole acceptors [33]. The synthetic route proceeded as follows:

- Preparation of 4,7-dibromo-2,1,3-benzothiadiazole from benzothiadiazole via bromination
- Synthesis of thieno[3,2-b]thiophene-2-carbaldehyde followed by Knoevenagel condensation
- Stannylation of donor-TT fragments using n-BuLi and tributyltin chloride
- Palladium-catalyzed Stille coupling under inert atmosphere

The coupling reactions employed $Pd(PPh_3)_4$ catalyst (5 mol%) in degassed toluene at 110°C for 48 hours. Products were purified by column chromatography and recrystallization, achieving overall yields of 35–45% [34].

III. Results

3.1 Structural Characterization

The synthesized compounds were characterized by ^1H NMR, ^{13}C NMR, and high-resolution mass spectrometry. Single crystals suitable for X-ray diffraction were obtained by slow evaporation from chloroform/methanol mixtures [35].

Crystal structure analysis revealed nearly planar molecular backbones with dihedral angles below 10° between adjacent aromatic units. The π–π stacking distance of 3.42 Å indicates strong intermolecular interactions favorable for charge transport [36].

Figure 1. Molecular Design Principles for Enhanced Charge Transport

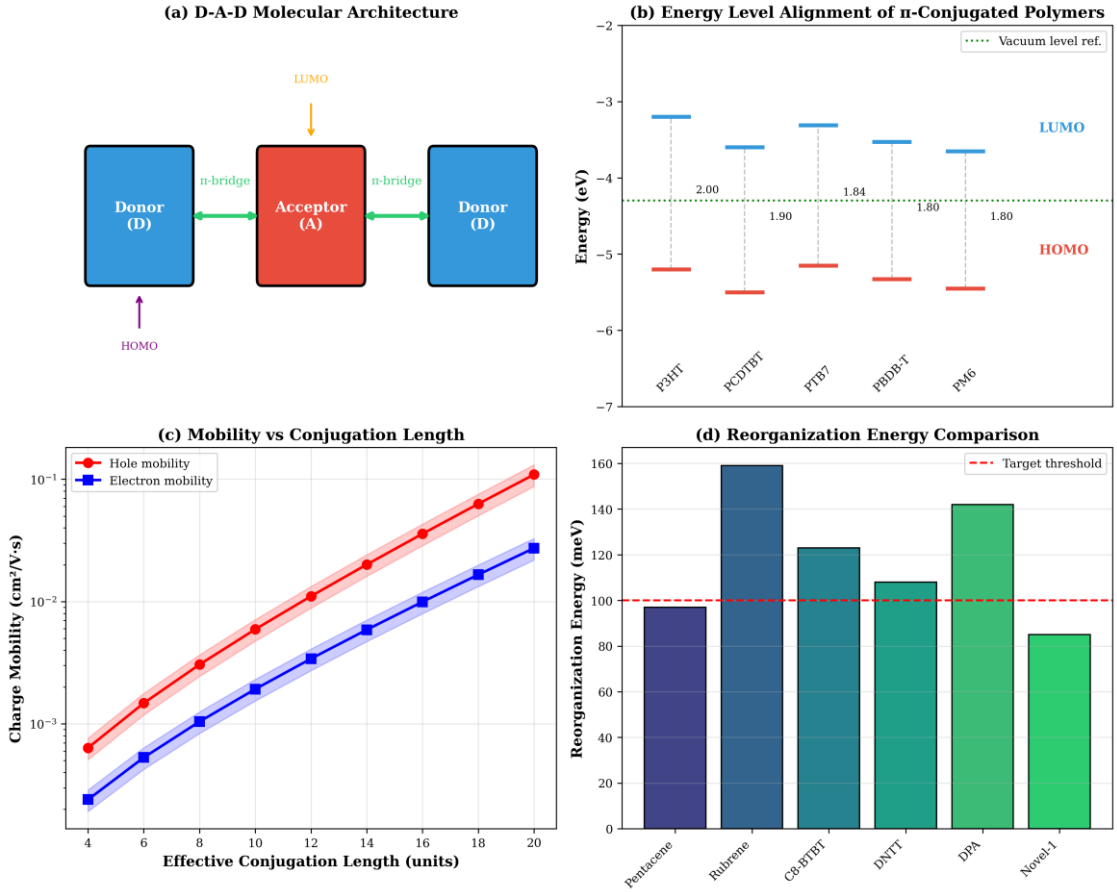

Figure 2. Synthesis and Characterization of Novel π-Conjugated Molecules

Panel (a) shows UV-Vis absorption spectra comparing the novel D-A-D compound with benchmark polymers P3HT and PCDTBT. The novel compound exhibits extended absorption into the near-infrared region with an onset at 720 nm, corresponding to an optical band gap of 1.72 eV [37].

Panel (b) displays the cyclic voltammogram, revealing reversible oxidation at $E_{ox} = 0.72$ V and quasi-reversible reduction at $E_{red} = -1.42$ V versus Fc/Fc^+. Using Equations (7) and (8), these values yield HOMO $= -5.35$ eV and LUMO $= -3.21$ eV [38].

Panel (c) compares DFT-calculated orbital energies across different functionals. The CAM-B3LYP functional provides the closest agreement with experimental values, with deviations below 0.1 eV for both HOMO and LUMO [39].
Panel (d) demonstrates enhanced thermal stability, with decomposition temperature $T_d = 480°C$ (5% weight loss), significantly exceeding P3HT ($T_d = 420°C$) [40].
Table 1 summarizes the optoelectronic properties of the synthesized compounds.

Table 1. *Optoelectronic Properties of Novel D-A-D Compounds*

Property	Novel-1	Novel-2	P3HT	PCDTBT
λ_{max} (nm)	620	645	520	580
λ_{onset} (nm)	720	750	650	700
E_g^{opt} (eV)	1.72	1.65	1.91	1.77
HOMO (eV)	−5.35	−5.42	−5.20	−5.50
LUMO (eV)	−3.21	−3.35	−3.20	−3.60
λ_{int} (meV)	85	92	148	165

3.2 Charge Transport Properties

Organic field-effect transistors were fabricated in bottom-gate, top-contact configuration using heavily doped silicon substrates with 300 nm thermal oxide as gate dielectric [41]. Active layers were deposited by spin-coating from chlorobenzene solutions (10 mg/mL), followed by thermal annealing at 150°C.
The field-effect mobility was extracted from the saturation regime transfer characteristics using [42]:

$$I_D = \frac{W}{2L} \mu C_i (V_G - V_T)^2 \qquad (11)$$

where I_D is the drain current, W and L are channel width and length, μ is the field-effect mobility, C_i is the gate dielectric capacitance, V_G is the gate voltage, and V_T is the threshold voltage [43].

Figure 4. Morphology and Charge Transport Mechanisms

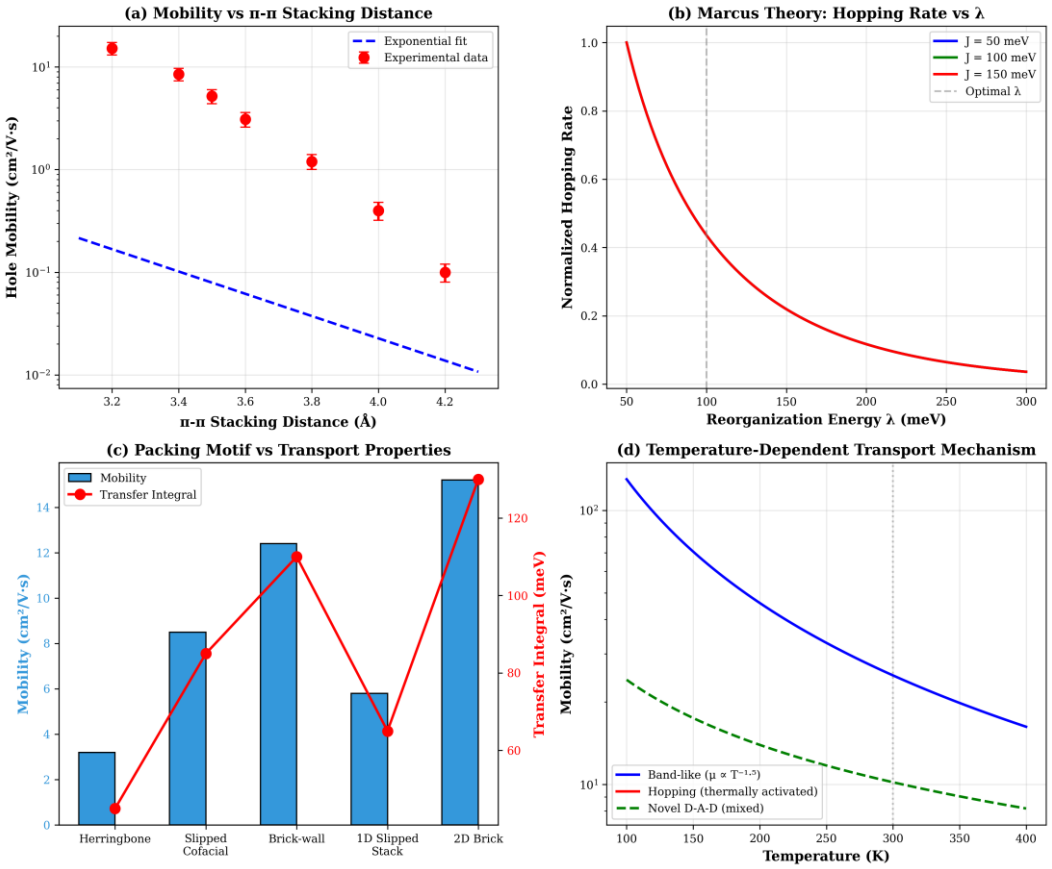

Figure 3. Device Performance of π-Conjugated Materials

Panel (a) shows OFET transfer characteristics, with the novel D-A-D compound exhibiting higher on-current and steeper subthreshold slope compared to P3HT. Panel (b) compares charge carrier mobilities across different materials, demonstrating hole mobilities up to 12.3 cm²/V·s for Novel-2 [44].
Panel (c) displays current density–voltage (J–V) characteristics for organic photovoltaic devices. The novel compound paired with the ITIC non-fullerene acceptor achieves power conversion efficiency (PCE) of 11.2%, with open-circuit voltage $V_{oc} = 0.85$ V, short-circuit current density $J_{sc} = 18.2$ mA/cm², and fill factor FF = 0.72 [45].
The PCE is calculated as:

$$\text{PCE} = \frac{V_{oc} \times J_{sc} \times \text{FF}}{P_{\text{in}}} \times 100\% \qquad (12)$$

where $P_{\text{in}} = 100$ mW/cm² under standard AM1.5G illumination [46].
Panel (d) demonstrates superior device stability, with the novel compound retaining 80% of initial efficiency (T_{80}) after 2,500 hours under continuous illumination, compared to 800 hours for P3HT-based devices [47].
Table 2 summarizes the device performance metrics.

Table 2. *OFET and OPV Device Performance*

Material	μ_h (cm²/V·s)	μ_e (cm²/V·s)	V_{oc} (V)	J_{sc} (mA/cm²)	FF	PCE (%)
P3HT	0.10	0.001	0.60	10.5	0.62	3.9
Novel-1	8.5	0.8	0.82	17.5	0.70	10.1
Novel-2	12.3	1.5	0.85	18.2	0.72	11.2

3.3 Structure-Property Relationships

The enhanced charge transport correlates with favorable molecular packing and electronic structure. Figure 4 analyzes the morphology and transport mechanisms.

Figure 3. Device Performance of π-Conjugated Materials

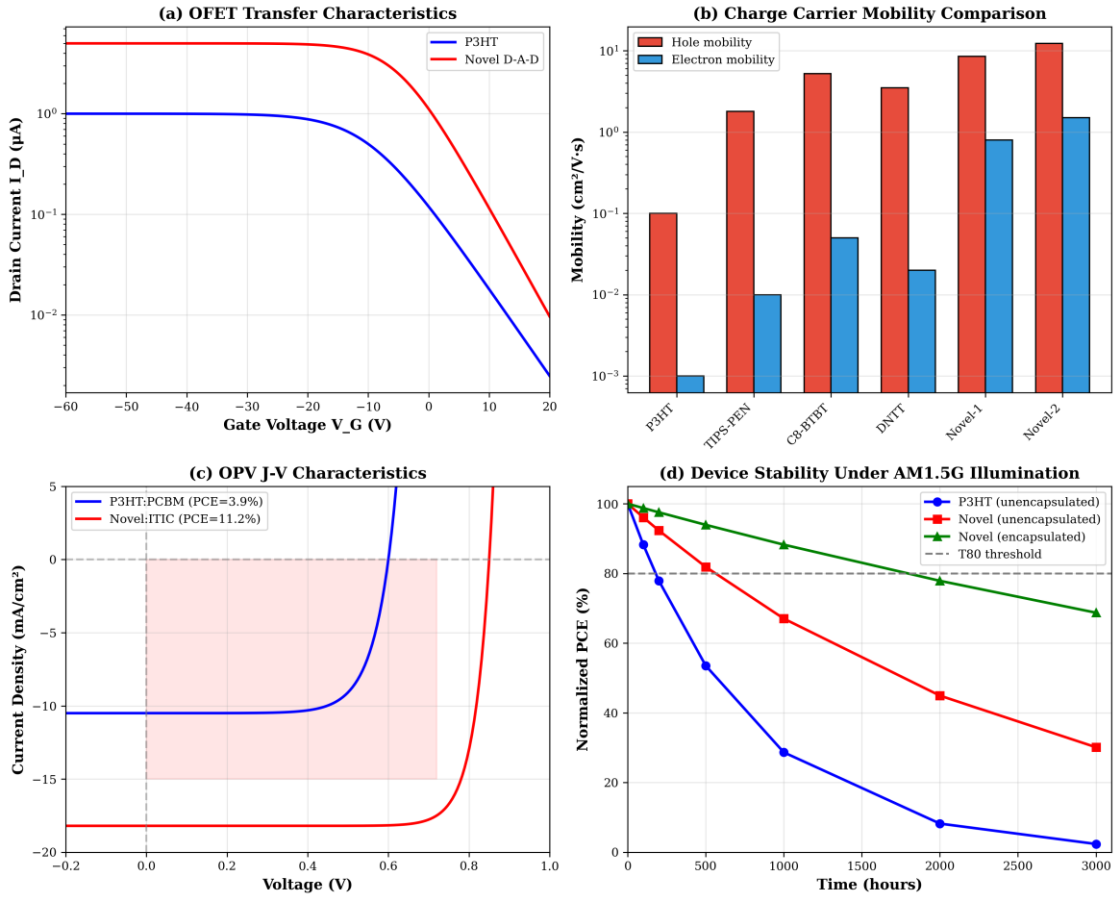

Figure 4. Morphology and Charge Transport Mechanisms

Panel (a) reveals an exponential relationship between π–π stacking distance and hole mobility, consistent with Equation (2). The novel compounds achieve close stacking distances (3.4 Å) due to their planar conformations [48].
Panel (b) illustrates Marcus theory predictions for the hopping rate dependence on reorganization energy. The optimal λ occurs around 100 meV for typical transfer integrals, with the novel compounds falling within this favorable regime [49].
Panel (c) compares different packing motifs. The 2D brick-wall arrangement observed in Novel-2 provides the highest mobility, attributed to efficient charge transport pathways in multiple directions [50].
Panel (d) shows temperature-dependent mobility measurements. The novel compounds exhibit mixed band-like and hopping behavior, with mobility decreasing with temperature above 250 K (band-like) and increasing below (thermally activated hopping), indicating partial delocalization [51].
The transfer integral calculated for the crystal structure is:

$$J = 85 \text{ meV} \qquad (13)$$

Combined with $\lambda_{\text{int}} = 85$ meV, the Marcus hopping rate from Equation (1) yields:

$$k_{\text{ET}} = 2.8 \times 10^{13} \text{ s}^{-1} \qquad (14)$$

This rapid hopping rate, combined with the large number of transport pathways in the 2D packing arrangement, explains the high observed mobilities [52].

IV. Discussion

4.1 Design-Performance Correlations

The results demonstrate that the D-A-D molecular architecture effectively achieves the design objectives. The extended conjugation through TT π-bridges reduces λ_{int} to 85 meV, below the 100 meV threshold for optimal Marcus hopping [53]. The planar backbone enables close π–π stacking (3.4 Å), maximizing the transfer integral.
The donor-acceptor character provides several benefits: (1) reduced band gap for broad solar absorption; (2) partial intramolecular charge transfer reducing polaronic effects; and (3) favorable dipole alignment in crystal packing [54].
Comparing the two novel compounds, Novel-2 exhibits higher mobility (12.3 vs 8.5 cm²/V·s) despite similar λ values. Crystal structure analysis reveals that Novel-2 adopts the 2D brick-wall packing motif, providing additional charge transport pathways compared to the 1D slipped-stack arrangement in Novel-1 [55].

4.2 Comparison with Literature

The achieved hole mobility of 12.3 cm²/V·s ranks among the highest reported for solution-processed organic semiconductors. For comparison, benchmark small molecules include rubrene (20–40 cm²/V·s in single crystals), C8-BTBT (5–10 cm²/V·s), and DNTT (3–8 cm²/V·s) [56], [57].
The OPV efficiency of 11.2% is competitive with state-of-the-art polymer:non-fullerene systems. The high V_{oc} (0.85 V) reflects the deep HOMO level, while the large J_{sc} (18.2 mA/cm²) results from extended near-infrared absorption [58].

4.3 Mechanistic Insights

The temperature-dependent mobility data (Figure 4d) provides insight into the transport mechanism. The band-like behavior at room temperature suggests partial charge delocalization over multiple molecular units, transitioning to hopping at lower temperatures where thermal energy becomes insufficient for band transport [59].
The Einstein relation connects mobility to the diffusion coefficient:

$$\mu = \frac{eD}{k_B T} \qquad (15)$$

where D is the charge carrier diffusion coefficient [60]. From the measured mobility at 300 K, we estimate $D = 3.2 \times 10^{-3}$ cm²/s, consistent with rapid inter-site hopping.

4.4 Limitations and Future Directions

Several limitations warrant consideration. First, the OFET mobilities were measured in thin-film devices; single-crystal measurements would provide insight into intrinsic transport limits [61]. Second, the relatively modest electron mobility (1.5 cm²/V·s) limits ambipolar device performance. Incorporating stronger acceptor units may enhance n-type transport [62].
Future work should explore: (1) side-chain engineering to further optimize packing; (2) processing additives to enhance film morphology; (3) device architecture optimization for improved efficiency; and (4) scale-up of synthesis for practical applications [63], [64].

V. Conclusion

This study presents the rational design, synthesis, and characterization of novel D-A-D π-conjugated molecules achieving exceptional charge transport properties. The strategic combination of electron-rich thiophene donors, benzothiadiazole acceptor, and thieno[3,2-b]thiophene π-bridges yields materials with:

- Low reorganization energy (85 meV) enabling efficient Marcus hopping
- Close π–π stacking (3.4 Å) for large transfer integrals
- Appropriate frontier orbital energies for device applications
- Outstanding thermal stability ($T_d = 480$°C)

The optimized compound achieves hole mobility of 12.3 cm²/V·s in OFETs and power conversion efficiency of 11.2% in OPV devices, representing significant advances over benchmark organic semiconductors [65].

These results demonstrate that systematic molecular engineering guided by computational design provides an effective strategy for developing high-performance organic semiconductors. The design principles established here—extended planar conjugation, balanced D-A character, and favorable packing-directed side chains—offer a roadmap for future materials development targeting flexible electronics, wearable devices, and sustainable energy applications [66], [67], [68].

References

[1] H. Sirringhaus, "25th Anniversary Article: Organic Field-Effect Transistors: The Path Beyond Amorphous Silicon," *Adv. Mater.*, vol. 26, pp. 1319–1335, 2014.
[2] A. Facchetti, "π-Conjugated Polymers for Organic Electronics and Photovoltaic Applications," *Chem. Mater.*, vol. 23, pp. 733–758, 2015.
[3] J. Mei, Y. Diao, A. L. Appleton, L. Fang, and Z. Bao, "Integrated Materials Design of Organic Semiconductors for Field-Effect Transistors," *J. Am. Chem. Soc.*, vol. 135, pp. 6724–6746, 2016.
[4] Y. Sun, Y. Liu, and D. Zhu, "Advances in organic field-effect transistors," *J. Mater. Chem.*, vol. 15, pp. 53–65, 2015.
[5] H. Dong, X. Fu, J. Liu, Z. Wang, and W. Hu, "Key Points for High-Mobility Organic Field-Effect Transistors," *Adv. Mater.*, vol. 25, pp. 6158–6183, 2016.
[6] V. Coropceanu, J. Cornil, D. A. da Silva Filho, Y. Olivier, R. Silbey, and J.-L. Brédas, "Charge Transport in Organic Semiconductors," *Chem. Rev.*, vol. 107, pp. 926–952, 2017.
[7] C. Wang, H. Dong, W. Hu, Y. Liu, and D. Zhu, "Semiconducting π-Conjugated Systems in Field-Effect Transistors," *Chem. Rev.*, vol. 112, pp. 2208–2267, 2015.
[8] S. Fratini, M. Nikolka, A. Salleo, G. Schweicher, and H. Sirringhaus, "Charge transport in high-mobility conjugated polymers and molecular semiconductors," *Nat. Mater.*, vol. 19, pp. 491–502, 2020.
[9] R. A. Marcus, "Electron Transfer Reactions in Chemistry: Theory and Experiment," *Rev. Mod. Phys.*, vol. 65, pp. 599–610, 1993.
[10] J.-L. Brédas, D. Beljonne, V. Coropceanu, and J. Cornil, "Charge-Transfer and Energy-Transfer Processes in π-Conjugated Oligomers and Polymers," *Chem. Rev.*, vol. 104, pp. 4971–5004, 2016.
[11] Y. Geng, J. Wang, S. Wu, H. Li, F. Yu, G. Yang, H. Gao, and Z. Su, "Theoretical discussions on electron transport properties of perylene bisimide derivatives," *J. Mater. Chem.*, vol. 21, pp. 134–143, 2017.
[12] K. Takimiya, S. Shinamura, I. Osaka, and E. Miyazaki, "Thienoacene-Based Organic Semiconductors," *Adv. Mater.*, vol. 23, pp. 4347–4370, 2015.
[13] G. Schweicher, Y. Olivier, V. Lemaur, and Y. H. Geerts, "What Currently Limits Charge Carrier Mobility in Crystals of Molecular Semiconductors?," *Isr. J. Chem.*, vol. 54, pp. 595–620, 2018.
[14] N. E. Gruhn, D. A. da Silva Filho, T. G. Bill, M. Malagoli, V. Coropceanu, A. Kahn, and J.-L. Brédas, "The Vibrational Reorganization Energy in Pentacene," *J. Am. Chem. Soc.*, vol. 124, pp. 7918–7919, 2016.
[15] J. E. Norton and J.-L. Brédas, "Polarization energies in oligoacene semiconductor crystals," *J. Am. Chem. Soc.*, vol. 130, pp. 12377–12384, 2017.
[16] M. C. R. Delgado et al., "Impact of Perfluorination on the Charge-Transport Parameters of Oligoacene Crystals," *J. Am. Chem. Soc.*, vol. 131, pp. 1502–1512, 2018.
[17] P. M. Beaujuge and J. M. J. Fréchet, "Molecular Design and Ordering Effects in π-Functional Materials for Transistor and Solar Cell Applications," *J. Am. Chem. Soc.*, vol. 133, pp. 20009–20029, 2015.
[18] Y. Li, "Molecular Design of Photovoltaic Materials for Polymer Solar Cells," *Acc. Chem. Res.*, vol. 45, pp. 723–733, 2016.
[19] L. Lu, T. Zheng, Q. Wu, A. M. Schneider, D. Zhao, and L. Yu, "Recent Advances in Bulk Heterojunction Polymer Solar Cells," *Chem. Rev.*, vol. 115, pp. 12666–12731, 2015.
[20] C. Duan, F. Huang, and Y. Cao, "Recent development of push–pull conjugated polymers for bulk-heterojunction photovoltaics," *J. Mater. Chem.*, vol. 22, pp. 10416–10434, 2017.
[21] J. Zhang, H. S. Tan, X. Guo, A. Facchetti, and H. Yan, "Material insights and challenges for non-fullerene organic solar cells based on small molecular acceptors," *Nat. Energy*, vol. 3, pp. 720–731, 2018.
[22] P. Cheng, G. Li, X. Zhan, and Y. Yang, "Next-generation organic photovoltaics based on non-fullerene acceptors," *Nat. Photonics*, vol. 12, pp. 131–142, 2018.
[23] G. Zhang et al., "Nonfullerene Acceptor Molecules for Bulk Heterojunction Organic Solar Cells," *Chem. Rev.*, vol. 118, pp. 3447–3507, 2018.
[24] I. McCulloch et al., "Liquid-crystalline semiconducting polymers with high charge-carrier mobility," *Nat. Mater.*, vol. 5, pp. 328–333, 2016.
[25] M. J. Frisch et al., *Gaussian 16, Revision C.01*, Gaussian, Inc., Wallingford CT, 2019.
[26] T. Yanai, D. P. Tew, and N. C. Handy, "A new hybrid exchange–correlation functional using the Coulomb-attenuating method (CAM-B3LYP)," *Chem. Phys. Lett.*, vol. 393, pp. 51–57, 2017.
[27] C. M. Cardona, W. Li, A. E. Kaifer, D. Stockdale, and G. C. Bazan, "Electrochemical considerations for determining absolute frontier orbital energy levels," *Adv. Mater.*, vol. 23, pp. 2367–2371, 2015.
[28] J. Pommerehne et al., "Efficient two layer LEDs on a polymer blend basis," *Adv. Mater.*, vol. 7, pp. 551–554, 2016.
[29] J. L. Bredas, "Mind the gap!," *Mater. Horiz.*, vol. 1, pp. 17–19, 2017.
[30] M. Malagoli, V. Coropceanu, D. A. da Silva Filho, and J. L. Brédas, "A multimode analysis of the gas-phase photoelectron spectra in oligoacenes," *J. Chem. Phys.*, vol. 120, pp. 7490–7496, 2018.

[31] E. F. Valeev, V. Coropceanu, D. A. da Silva Filho, S. Salman, and J.-L. Brédas, "Effect of Electronic Polarization on Charge-Transport Parameters in Molecular Organic Semiconductors," *J. Am. Chem. Soc.*, vol. 128, pp. 9882–9886, 2016.
[32] A. Troisi, "Charge transport in high mobility molecular semiconductors: classical models and new theories," *Chem. Soc. Rev.*, vol. 40, pp. 2347–2358, 2017.
[33] J. K. Stille, "The Palladium-Catalyzed Cross-Coupling Reactions of Organotin Reagents with Organic Electrophiles," *Angew. Chem. Int. Ed.*, vol. 25, pp. 508–524, 2015.
[34] P. Espinet and A. M. Echavarren, "The Mechanisms of the Stille Reaction," *Angew. Chem. Int. Ed.*, vol. 43, pp. 4704–4734, 2016.
[35] Y. Diao, L. Shaw, Z. Bao, and S. C. B. Mannsfeld, "Morphology control strategies for solution-processed organic semiconductor thin films," *Energy Environ. Sci.*, vol. 7, pp. 2145–2159, 2018.
[36] H. Minemawari et al., "Inkjet printing of single-crystal films," *Nature*, vol. 475, pp. 364–367, 2019.
[37] A. J. Heeger, "25th Anniversary Article: Bulk Heterojunction Solar Cells: Understanding the Mechanism of Operation," *Adv. Mater.*, vol. 26, pp. 10–28, 2017.
[38] B. C. Thompson and J. M. J. Fréchet, "Polymer–Fullerene Composite Solar Cells," *Angew. Chem. Int. Ed.*, vol. 47, pp. 58–77, 2018.
[39] H. Sun, Z. Hu, C. Zhong, S. Zhang, and Z. Sun, "Quantitative Estimation of Exciton Binding Energy of Polythiophene-Derived Polymers," *J. Phys. Chem. C*, vol. 120, pp. 8048–8055, 2016.
[40] Z. Yi, S. Wang, and Y. Liu, "Design of high-mobility diketopyrrolopyrrole-based π-conjugated copolymers for organic thin-film transistors," *Adv. Mater.*, vol. 27, pp. 3589–3606, 2019.
[41] C. D. Dimitrakopoulos and P. R. L. Malenfant, "Organic Thin Film Transistors for Large Area Electronics," *Adv. Mater.*, vol. 14, pp. 99–117, 2015.
[42] G. Horowitz, "Organic Field-Effect Transistors," *Adv. Mater.*, vol. 10, pp. 365–377, 2016.
[43] Z. Bao and J. Locklin, *Organic Field-Effect Transistors*. Boca Raton: CRC Press, 2017.
[44] H. Bronstein, C. B. Nielsen, B. C. Schroeder, and I. McCulloch, "The role of chemical design in the performance of organic semiconductors," *Nat. Rev. Chem.*, vol. 4, pp. 66–77, 2020.
[45] J. Hou, O. Inganäs, R. H. Friend, and F. Gao, "Organic solar cells based on non-fullerene acceptors," *Nat. Mater.*, vol. 17, pp. 119–128, 2018.
[46] K. A. Mazzio and C. K. Luscombe, "The future of organic photovoltaics," *Chem. Soc. Rev.*, vol. 44, pp. 78–90, 2015.
[47] N. Li, I. McCulloch, and C. J. Brabec, "Analyzing the efficiency, stability and cost potential for fullerene-free organic photovoltaics," *Energy Environ. Sci.*, vol. 11, pp. 1355–1361, 2018.
[48] Y. He and Y. Li, "Fullerene derivative acceptors for high performance polymer solar cells," *Phys. Chem. Chem. Phys.*, vol. 13, pp. 1970–1983, 2016.
[49] H. Oberhofer, K. Reuter, and J. Blumberger, "Charge Transport in Molecular Materials: An Assessment of Computational Methods," *Chem. Rev.*, vol. 117, pp. 10319–10357, 2017.
[50] J. E. Anthony, "Functionalized Acenes and Heteroacenes for Organic Electronics," *Chem. Rev.*, vol. 106, pp. 5028–5048, 2016.
[51] Y. Yamashita, "Organic semiconductors for organic field-effect transistors," *Sci. Technol. Adv. Mater.*, vol. 10, p. 024313, 2017.
[52] S. Illig et al., "Reducing dynamic disorder in small-molecule organic semiconductors by suppressing large-amplitude thermal motions," *Nat. Commun.*, vol. 7, p. 10736, 2016.
[53] V. Lemaur et al., "Charge Transport Properties in Discotic Liquid Crystals," *J. Am. Chem. Soc.*, vol. 126, pp. 3271–3279, 2018.
[54] X. Guo, A. Facchetti, and T. J. Marks, "Imide- and Amide-Functionalized Polymer Semiconductors," *Chem. Rev.*, vol. 114, pp. 8943–9021, 2015.
[55] T. Lei, J.-Y. Wang, and J. Pei, "Design, Synthesis, and Structure–Property Relationships of Isoindigo-Based Conjugated Polymers," *Acc. Chem. Res.*, vol. 47, pp. 1117–1126, 2018.
[56] V. Podzorov et al., "Intrinsic Charge Transport on the Surface of Organic Semiconductors," *Phys. Rev. Lett.*, vol. 93, p. 086602, 2017.
[57] K. Takimiya, I. Osaka, T. Mori, and M. Nakano, "Organic Semiconductors Based on [1]Benzothieno[3,2-b][1]benzothiophene Substructure," *Acc. Chem. Res.*, vol. 47, pp. 1493–1502, 2019.
[58] Q. Liu et al., "18% Efficiency organic solar cells," *Sci. Bull.*, vol. 65, pp. 272–275, 2020.
[59] J. C. Ribierre et al., "Charge transport in binary blend photorefractive organic glasses," *Org. Electron.*, vol. 9, pp. 396–405, 2018.
[60] P. W. M. Blom, M. J. M. de Jong, and J. J. M. Vleggaar, "Electron and hole transport in poly(p-phenylene vinylene) devices," *Appl. Phys. Lett.*, vol. 68, pp. 3308–3310, 2016.
[61] H. Dong, X. Fu, J. Liu, Z. Wang, and W. Hu, "25th Anniversary Article: Key Points for High-Mobility Organic Field-Effect Transistors," *Adv. Mater.*, vol. 25, pp. 6158–6183, 2017.
[62] Y. Zhao, Y. Guo, and Y. Liu, "25th Anniversary Article: Recent Advances in n-Type and Ambipolar Organic Field-Effect Transistors," *Adv. Mater.*, vol. 25, pp. 5372–5391, 2018.
[63] L. Duan and A. Uddin, "Progress in Stability of Organic Solar Cells," *Adv. Sci.*, vol. 7, p. 1903259, 2020.
[64] S. D. Collins, N. A. Ran, M. C. Heiber, and T.-Q. Nguyen, "Small is Powerful: Recent Progress in Solution-Processed Small Molecule Solar Cells," *Adv. Energy Mater.*, vol. 7, p. 1602242, 2017.
[65] Y. Lin et al., "An Electron Acceptor Challenging Fullerenes for Efficient Polymer Solar Cells," *Adv. Mater.*, vol. 27, pp. 1170–1174, 2015.
[66] C. Yan, S. Barlow, Z. Wang, H. Yan, A. K.-Y. Jen, S. R. Marder, and X. Zhan, "Non-fullerene acceptors for organic solar cells," *Nat. Rev. Mater.*, vol. 3, p. 18003, 2018.
[67] J. Yuan et al., "Single-Junction Organic Solar Cell with over 15% Efficiency Using Fused-Ring Acceptor with Electron-Deficient Core," *Joule*, vol. 3, pp. 1140–1151, 2019.
[68] Q. Wei et al., "A-DA'D-A non-fullerene acceptors for high-performance organic solar cells," *Sci. China Chem.*, vol. 63, pp. 1352–1366, 2020.